Comparison of Goldstone and Magellan Radar Data in the Equatorial Plains of Venus

JEFFREY J. PLAUT[1] AND RAYMOND E. ARVIDSON[2]

Goldstone radar observations of the equatorial plains of Venus provide complementary information to that obtained by Magellan. Different radar scattering mechanisms dominate each system, leading to a sampling of different surface properties. Comparison of image data and derived parameters indicate that (1) relatively high dielectric con stants on impact-related parabolic features are detected in Gold stone backscatter, Magellan reflectivity, and Magellan emissivity data; the dielectric effects arc overwhelmed by roughness-related signatures in Magellan synthetic aperature radar (SAR) data, (2) lava flows in Navka Planitia ahow dielectric variations both among and within flows; higher dielectric constants on the perimeter of some flows may be due to a decrease in vesicularity, (3) some volcanic domes are relatively smooth at the wavelength scale and probably consist of low-density deposits, (4) comparisons of Magellan SAR data with rough surface scattering models and SAR data of terrestrial surfaces indicate that the roughness characteristics of the equatorial plains surfaces arc comparable to modified terrestrial lava flows, and (5) scattering properties of an equatorial "ridge belt" structure suggest highly weathered or soil - dominated surfaces.

INTRODUCTION

The Goldstone Solar System Radar has acquired radar image and altimetry observations of the surface of Venus since 1972 [Rumsey et al., 1974; Jurgens et al., 1980, 1988a,b] (see Arvidson et al. [1990] for a review). The Goldstone observations are unique among existing Venus radar data sets in that they are obtained at very small incidence angles (00-70), and include high resolution (1- 10 km) altimetry measurements coregistered to the backscatter images. The controls on radar backscatter at small incidence angles are quite different than at the larger angles used for Magellan synthetic aperature radar (SAR) imaging. In this paper, we (1) consider the effects of the differing viewing geometries used by Goldstone and Magellan on radar scattering behavior, (2) compare images from the two systems, demonstrating the complementary nature of the observations, and (3) compare quantitative data from the two systems, including the Magellan altimetry and radiometry experiments, to more fully characterize the radar scattering properties of selected surfaces in the equatorial plains.

The Goldstone backscatter and altimetry data were obtained during periods of inferior conjunction, and are thus limited in longitudinal coverage to the area between approximately 260°E and 30°E (through O°). The observations are similarly limited in latitude to regiona near the sub-Earth point, approximately between 150N and 15°S latitude. The locations of Goldstone data obtained since 1972 are shown on a Magellan SAR mosiac in Figure 1. Gaps near the center of the Magellan mosaic are due to abbbreviated, thermally constrained mapping passes in the latter phases of the first mapping cycle. The study area includes parts of Phoebe and Eistla regiones and parts of Guinevere, Navka, and Tinatin planitiae. Major structural features include Devana Chasma (the southern extension of the Beta Regio rift system) at 288°E longitude and the -1000 km diameter corona Heng-O at 353°E longitude [Plaut et al., 1990; Squyres et al., this issue].

RADAR SCATTERING CONSIDERATIONS

The Goldstone and Magellan radar imaging systems operate at the same wavelength (S-band, ~12.6 cm) but differ in resolution, incidence angle, and polarization. Observational parameters of the two systems are listed in Table 1. Resolution in Goldstone data has been improved from 5-10 km in early data to near 1 km in data acquired since 1986 [Jurgens et al., 1988a]. Magellan SAR resolution is set to 120 m along-track and varies from 100 m to 360 m across-track, Incidence angles for tbc Goldstone Venus observations range from nadir to about 7°, while Magellan SAR cycle 1 incidence angles range from 17° at high latitudes to 45° in the equatorial region under consideration here, The Goldstone system transmits a circularly polarized signal and receives echoes in the opposite sense circular ("expected") polarization. Polarization for Magellan is horizontal transmit and receive (HH).

The differences in observational parameters of the two systems lead to significant differences in the effects of surface characteristics on the backscattered signals. At the small incidence angles and cross-circular polarization of the Goldstone observations, backscatter is dominated by the quasi-specular scattering mechanism [Hagfors, 1970]. Backscatter strength in this regime is strongly dependent on local incidence angle and is thus highly sensitive to topographic variations. In addition, surface undulations at states many multiples of the wavelength (meters to tens of meters) tend to scatter energy in directions other than the backscatter direction. Extensive flat areas will therefore appear bright in Goldstone images, while areas with a high value of rms slope will appear dark. Finally, backscatter in the quasi-specular regime, as modelled by Hagfors [1970], is proportional to the Fresnel reflection coefficient of the surface material.

During its first mapping cycle, the Magellan SAR observed the equatorial regions at incidence angles between 40° and 45°. Backscatter strength in this regime is dominated by surface roughness elements comparable in size to the scale of the 12.6-cm wavelength. In addition, surfaces with large blocks that have facets oriented normal to the incident beam may also appear bright at these incidence angles [Plaut, 1991]. The dependence of backscatter on incidence angle is weak at large angles, but steep topographic slopes are detectable. Variations in dielectric constant (also expressed as Fresnel reflectivity) can affect backscatter strength at large incidence angles, but for the range of dielectric constants expected in Venus' plains regions, this effect is overwhelmed by roughness variations.

The Magellan radar obtains data in two additional modes, altimetry and radiometry. The nadir-pointing altimeter is used as a ranging device, but echoes arc also analyzed for power, dispersion in the time domain, and frequency content [Pettengill et al., 1991, this issue]. Estimates of Fresnel reflectivity and rms slope are obtained from this analysis for altimetric resolution cells averaging ~10 km in diameter. Between reception of SAR echo bursts, the high-gain antenna is also used to detect passively emitted radiation from the planet's surface at emission angles comparable to the SAR incidence angles, These data are reduced to values of emissivity at a footprint size of -20 km [Pettengill et al., 1991, this issue]. Emissivity generally behaves as the unit complement of

Fresnel reflectivity (i.e., ρ_0=1 -e), providing independent checks for the two determinations.

The full ensemble of Magellan and Goldstone measurements can be used to characterize the scattering properties of areas of the planet where there is overlap in the data sets. The set of parameters is useful for understanding the physical surface characteristics that produce a particular radar signature. The parameters include values of specific radar cross section, σ^0, at small (Goldstone) and large (Magellan) incidence angles. In addition, determinations of Fresnel reflectivity and rms slope made from calibrated Goldstone data [Plaut et al., 1990] can be compared with estimates derived from Magellan altimetry measurements. Other parameters that relate to physical surface properties are Magellan emissivity and Fresnel reflectivity corrected for diffuse scatter [Pettengill et al., 1988]. Table 2 provides the complete set of properties for three surfaces to be discussed later in this paper. Goldstone data provide important complementary information to the Magellan data sets because they include calibrated image and altimetry data at higher resolution than Magellan altimetry, as well as measurements of specific cross section, σ^0, at incidence angles -40° smaller than the Magellan SAR.

COMPARISON OF IMAGE DATA

With their high spatial resolution, Magellan SAR image data greatly clarify the nature of features that have appeared in Goldstone image data over the past 20 years. However, because of the different viewing geometries, Goldstone data are not merely superseded by Magellan but continue to provide complementary information about surface features. In this section, Goldstone and Magellan images arc compared, with an emphasis on explaining the physical mechanisms leading to differences and similarities in the appearance of features in the two data sets.

Heng-O Corona

The northeast portion of the corona structure Heng-O was imaged by Goldstone at a resolution of -1 km in 1988 [Plaut et al., 1990]. Magellan image and altimetry data have confirmed that Heng-O has many of the characteristics associated with coronae, including an annulus of concentric ridges and fractures, a peripheral trough, and an interior with both tectonically disrupted and volcanic structures [Squyres et al., this issue]. Figure 2 is a comparison of Goldstone and Magellan images for northeastern Heng-O and the adjacent plains. The high sensitivity to topography at small radar incidence angles is dramatically illustrated by the prominence of the northern inner scarp of the corona in the Goldstone image. The Magellan look direction is roughly parallel to the strike of much of the scarp, but the topographic enhancement is minor even in places where a significant component of the slope is perpendicular to the incident beam. Magellan altimetry confirm the 1-2 km of relief on this structure that was reported from Goldstone observations [Plaut et al., 1990]. Although the Goldstone altimetry data corresponding to this image (not shown here) are of uneven quality, the topographic sensitivity of the Goldstone image data emphasizes details of topography that are too subtle to be

dctectcd by the Magellan SAR and arc too small to be detected by the Magellan altimeter. For example, the southwest trending bright feature in the lower left of Figure 2a results from a decrease in local incidence angle duc to a partially radar-facing slope. Topographic details on this feature and other structures in the corona interior are not detected by the M agellan SAR or altimeter. An interesting geometric effect occurs in the Goldstone data on the impact crater Hellman (35 km diameter), near the center of the frame. Duc to the projection of the data in range space onto an assumed spherical surface, the higher elevation crater rim and ejects arc displaced slightly toward the subradar point, while the floor of the crater, which is several hundred meters deep, is displaced in the opposite direction.

An effect commonly encountered in comparing Goldstone and Magellan image data is a reversal of contrast relationships antong surfaces within a scene, For example, in Figure 2, a system of linear fractures in the lower portion of the scene appears bright in the Magellan image and dark in the Goldstone image. A similar relationship is seen on the ejects and flow deposits [Asimow and Wood, this issue] associated with Hellman crater and the ~18 km diameter crater Nadine in the upper right. Conversely, the floor of Hellman (displaced to the north of the ejecta) appears dark to M agellan and bright to Goldstone. These effects may be explained in terms of the effects of roughness on backscatter at the two different incidence angles. At Magellan incidence angles (43°-450 here), roughness at or near the wavelength scale dominates the backscatter, with rougher surfaces appearing bright. At Goldstone incidence angles (0.5°-4.5" here), roughness at the quasi-specular length scale dominates the backscatter, with smoother surfaces appearing bright. If the roughness characteristics of the surface are approximately scale-independent between the centimeter and decameter scale, then roughness variations will produce opposite effects in Magellan and Goldstone backscatter images. Such a roughness spectrum is to be expected for example, on crater ejecta, in which crater rim materials, ejects blocks and centimeter-scale debris produce surfaces that arc rougher than typical surrounding materials at the relevant length scales. A similar distribution of roughness elements is expected on fractured terrains, where decameter-scale ridges and troughs will have associated centimeter-scale talus and other debris.

High Dielectric Impact-Related Features

Approximately 5% of the impact craters identified from Magellan data have an associated low-emissivity, high-reflectivity west facing parabolic feature [Arvidson et al., 1991; Campbell et al., this issue]. Four of these features occur in the equatorial region covered by Goldstone image data. The surfaces arc characterized by emissivity values ~0.05 lower than the surroundings and corrected reflectivity values correspondingly higher than the surroundings. The features arc often indistinguishable from the surroundings in altimeter-derived rms slope data. In Magellan SAR images, the parabolic features are generally lower in backscatter than the surroundings. However, in many cases the signature is not visible in the SAR image, Conversely, many of the low SAR backscatter "halo" features [Campbell et al., this issue] have

little or no emissivity/reflectivity signature. These relationships suggest that the lower emissivity is not a roughness effect but rather an increase in dielectric constant due to differences in mineralogy or bulk density.

A fan-shaped parabolic feature, associated with Nadine crater, dominates the northern half of the Goldstone image of July 11, 1980 (Figure 3a). This image has a resolution of approximately 5 km, and was obtained with nearly the same subradar point as data in Figure 2. Magellan emissivity data for the area (Figure 3b) show the same fan-shaped feature, with values approximately 0.035 *lower than the* plains immediately to the east. A comparable increase is seen in Magellan corrected reflectivity between the feature and the plains. The feature is not prominent in Magellan SAR data (Figure 3c). Overall the area is lower in backscatter than the surroundings, but the eastern contact with the plains is indistinct, and the detailed structure of the feature is not well-correlated between the SAR and emissivity images.

In the absence of other information, the high backscatter signature of the fan-shaped feature in the Goldstone data of Figure 3a can be interpreted as a result of (1) topography that lowers the local incidence angle, (2) a low rms slope surface, (3) a smooth surface at the wavelength scale, and/or (4) a higher dielectric constant. Magellan altimetry data indicate that some of the brightness adjacent to the northern peripheral trough of Heng-O corona (saturated in Figure 3a) is probably a topographic effect. However. most of the surface has topographic gradients too low to explain the overall bright appearance. Magellan rms slope data show no signature corresponding to the feature. Furthermore, much of the feature appears bright at Goldstone incidence angles for which rms slope variations are expected to exert minimal control on backscatter. The wavelength-scale roughness may be slightly lower than the surroundings, as indicated by Magellan backscatter, but the poor correlation of details in the feature suggests that this is not the controlling mechanism in the Goldstone data. Details of the structure, especially its eastern margins, are well-correlated among Goldstone backscatter, Magellan emissivity, and Magellan corrected reflectivity, indicating that an increase in dielectric constant is the most likely source of the bright signature in the Goldstone image. Smoothness at the wavelength scale may further enhance the high backscatter in Goldstone data, while smoothness and high dielectric constants will tend to cancel each other out in Magellan backscatter. This may explain the sharpness of the *contacts* in Goldstone data relative to Magellan SAR data.

Volcanic Terrain in Navka Planitia

On the basis of analyses of Goldstone image data [Jurgens et al., 1980; Arvidson et al., 1990; Plaut, 1991], central Navka Planitia was identified as a region dominated by volcanic features. These included domelike hills, both in clusters and in isolated occurrences, and broad areas of contrasting radar backscatter, *commonly* displaying lobate margins or sinuous extensions. These features were interpreted as volcanic in origin, i.e., lava domes, shields, and flows. Magellan data, acquired near the end of the frost mapping cycle, have confirmed the volcanic nature of this region. A flow complex -800 km in

diameter is centered near 20N, 3 16“E (Figure 1, left center). Additional edifices and flows occur to the south and southwest, in art area imaged by Goldstone three-station interferometry in 1977 [Jurgens et al., 1980]. Figure 4 is a comparison of Goldstone and Magellan data for the area imaged by Goldstone on March 18, 1977.

Backscatter variations in Magellan SAR images of lava flows can usually be ascribed to differences in small-scale roughness. This is supported by the generally positive correlation of backscatter, rms slope and emissivity (an increase in emissivity being common on the roughest flow surfaces), There are, however, lava flows that display trends contrary to these, suggesting intrinsic dielectric differences and/or scale dependence in roughness characteristics. For example, some lava flows south of Sif Mons and other flows southwest of Heng-O corona have unusually low emissivities, and correspondingly higher reflectivities, suggesting that the backscatter contrast relative to the surroundings may be due in part to dielectric differences [Plaut et al., 1991; Campbell and Campbell, this issue]. There is a suggestion of changes in rms slope along the length of some flows, and with distance from the flow margin, but these variations are usually at too fine a scale to be identified in M agellan altimeter-derived data. Such variations may contain information on eruptive characteristics, such as effusion and cooling rates, lava viscosity, and transitions in flow morphology (e.g., pahoehoe to a'a).

Comparison of the Goldstone and Magellan images of Navka Planitia in Figure 4 shows examples of reversals in contrast relationships among surfaces, as well as examples of consistent contrast relationships. The contrast relationships on the flows in the northern half of the image are particularly complex. The brightest flows in the Goldstone image (arrow 1, Figure 4a) are intermediate in brightness in the Magellan data, but in both data sets these flows are brighter than the surrounding plains. A 70-km-diameter circular patch (arrow 3), dark in the Goldstone image, is seen to be a broad dome with a central pit in Magellan data. The dome shows minimal contrast in Magellan data relative to the adjacent flows in the south, while the contrast of the same surfaces in Goldstone data nearly spans the entire dynamic range, Two other patches within the bright flow unit, each -20-30 km in diameter, are dark in Goldstone data but are not discernible in the Magellan image, despite the higher resolution. An interesting effect is seen along the margins of two flow lobes near the center of the northern half of the frame (arrow 4). The lobes show little variation in backscatter in Magellan data. In Goldstone data, the backscatter is high on the proximal parts of the lobes, and decreases toward the distal portions. The margins, however, are marked by a continuous bright rim, -5-15 km wide, along the entire perimeter of the flow lobes. The bright margins have no corresponding signature in Magellan S AR data. The same effect is seen on a flow margin -500 km to the south, on Goldstone data from 1974 (not pictured).

What are the surface characteristics that produce such variable signatures in this volcanic terrain? Goldstone incidence angles for most of these features are in the 5°-70 range, for which differences in rms slopes are expected to have minimal effects on backscatter strength (the Hagfors

"crossover" region [Jurgens et al., 1980]). In the absence of large topographic gradients, backscatter variations in this Goldstone image are most likely due to differences in dielectric constant. Magellan emissiv ity and Fresnel reflectivity data for the Navka lava flows are consistent with this interpretation. Emissivity values for the bright and dark flows (arrows 1 and 2 on Figure 4a) are 0.738 and 0.808, respectively; corrected Fresnel reflectivities are 0.162 and 0.095, respectively. The lack of correlation between Magellan SAR backscatter and reflectivity measurements for these flows again indicates that roughness variations overwhelm dielectric variations in much of the Magellan SAR data. Assuming a negligible loss tangent, the reflectivities correspond to real dielectric constants of 5.5 and 3.6 for the bright and dark flows, respectively. These values are both consistent with laboratory measurements for rocks [Campbell and Ulrichs, 1969; Ulaby et al., 1990], although the lower value suggests a lower density rock (-2.0 g/cm^3). Bulk density differences among lava flows may result from differences in composition, degree of fracturing or vesicularity. The transitions in reflectivity observed within flows argues against a compositional control on the dielectric constant for these flows. Increased roughness at the centimeter scale should accompany surface fracturing, but Magellan SAR backscatter data do not consistently show the expected enhancement on lower reflectivity flows. We thus conclude that differences in vesicularity are primarily responsible for the observed variations in dielectric constant on the Navka lava flows. Radar characteristics of the 70 km dome (arrow 3 on Figure 4a) suggest a relatively smooth, low-density deposit, while the low-reflectivity flow (arrow 2) is rougher, with a similar low density. Increases in reflectivity observed on the perimeter of flows in the Goldstone data imply density differences possibly related to variable cooling histories within and at the margins of the flow.

COMPARISON OF SCATTERING PROPERTIES

A subset of the Goldstone image data set has been calibrated to absolute values of specific radar cross section, σ^0, [Plaut et al., 1990]. This allows direct quantitative comparison of radar measurements made by two reasonably well-calibrated radar systems under distinctly different viewing geometries. The set of parameters derived from these observations can be used to understand the physical surface characteristics that produce a particular radar signature. Three sets of these surface electrical properties are presented in Table 2. The surfaces include a plains area northeast of Heng-O corona, an adjacent surface within the low-emissivity impact-related feature, and a portion of a linear elevated structure (ridge belt) southwest of Heng-O. Values of Fresnel reflection coefficient, ρ_0, and rms slope are derived from the Goldstone data by fitting the Hagfors function to σ^0 values from a range of incidence angles. The ρ_0 values agree to within 0.015 with uncorrected p_0 values from Magellan. This comparison is appropriate because both determinations are based on near-nadir measurements, without correction for diffuse scattering effects. Goldstone estimates of rms slope are usually higher than those from Magellan altimetry. The discrepancy may result from the larger range of incidence angles (up to -15° in the equatorial regions) used in

the template matching procedure for Magellan data, although it is not clear that this would always lead to lower slope estimates.

Specific cross sections, σ^0, for the three surfaces are plotted in Figure 5. Also plotted are the Hagfors and Muhleman scattering laws for the average Venus surface, along with a small-perturbation model scattering function. The Hagfors function is based on planet-wide mean values of Magellan uncorrected Fresnel reflectivity and rms slope of 0.109 and 2.77°, respectively. The so-called Muhleman law [Pettengill et al., 1988] is an empirically derived average scattering function based on Pioneer Venus SAR observations. At incidence angles less than about 15°, the scattering behavior steepens relative to the Muhleman law, and the Hagfors function provides a better match to the observations. Contrast reversals, described in previous sections, are evident in Figure 5. The low-emissivity impact-related parabolic feature is brighter than the adjacent plains at small angles and darker than the plains at large angles. The -3 dB difference (- a factor of 2) in Goldstone σ^0 values for these two surfaces is consistent with the measured values of Fresnel reflectivity and emissivity (Table 2), The reversed contrast relationship at Magellan incidence angles indicates that differences in small-scale roughness overwhelm the dielectric differences for these two surfaces. The relatively low Goldstone σ^0 value for the ridge belt surface is also likely due to a lower dielectric constant, in view of the minimal effect of rms slope differences on σ^0 in the 5°-70 incidence angle range.

Data in Table 2 can be used to constrain the small-scale roughness characteristics of the surfaces. The small-perturbation model of rough surface scattering [Ulaby et al., 1982; van Zyl et al., 1987] predicts specific cross sections for a given dielectric constant and geometrical description of roughness characteristics. It has been found that the model is most successful in describing the full polarimetric scattering behavior of natural surfaces when an exponential distribution of surface heights is used [Plaut, 1991]. The geometrical parameters are the rrns surface height and the surface correlation length (a measure of the statistical independence of heights as a function of horizontal separation). Assuming a loss tangent of zero, the Fresnel reflection coefficients of Table 2 can be converted to dielectric constants. Using the Magellan σ^0 values, constraints on the rrns surface heights and correlation lengths are obtained by comparison with the small perturbation model, Model results indicate that σ^0 dependence on correlation length is weak. Rms height is the controlling parameter at these large incidence angles and with the inferred values of dielectric constant. Best model fits are obtained with the following values of dielectric constant (based on Magellan corrcctcd reflectivity) and rrns height, respectively: plains, 3.48, 2.4 cm; parabolic feature, 4.30, 1.9 cm; ridge belt, 2.89, 2.6 cm. The dielectric value for the plain.. unit is consistent with a rock-dominated surface, with a degree of roughness similar to highly modified lava flows in arid terrestrial environments [Plaut, 1991]. The higher dielectric value for the low-emissivity parabolic feature suggests a welded or soil-free surface, although the presence of conducting minerals should not be ruled out. The rms height value is similar to that found in terrestrial alluvial gravels and tephra deposits. Roughness characteristics on the ridge belt surface are again comparable to

modified terrestrial lava flows, but the low dielectric constant suggests a component of low density material. Using the density/dielectric relationship of Ulaby et al. [1990], a bulk density of -1.6 g/cm^3 is implied for the ridge belt materials, consistent with highly weathered or soil-dominated exposures.

Discussion and Conclusions

The above analyses have shown that by combining observations from the Magellan and Goldstone radar systems, an understanding of surface properties is obtained that would not be possible using data from either system alone. The additional information can be used to improve interpretations of the nature of geological surfaces and the processes that create and modify them, both in the areas covered by Goldstone and in similar terrains elsewhere on Venus.

In the Heng-O corona region, Goldstone data have revealed details of topography that are as yet inaccessible to Magellan. With same-side stereo imaging planned for later mapping cycles, much of this topographic detail may become available for geomorphological analyses. Contrast relationships between Goldstone and Magellan images of impact craters such as Hellman (Figure 2) show the scale independence of roughness on Venusian ejects deposits.

The low-emissivity, high-reflectivity parabolic features associated with many impact craters remain enigmatic, but Goldstone data appear to confirm that they are indeed characterized by higher dielectric constants than their surroundings. Whether this change in surface properties is a result of mineralogical or macroscale physical characteristics is yet to be determined. Multiple incidence angle and polarimetric coverage of these features in later mapping cycles may improve the understanding of the radar scattering mechanisms responsible for their unusual appearance (e.g., penetration, volume scattering, dielectric variations with depth, etc.).

Goldstone image data on lava flows reveal variations in dielectric properties among and within flows. The margins of a number of flows in the Navka Plaintia area appear to be more dense than the interiors, possibly because of lower vesicularity. A 70-km-diameter lava dome shows lower dielectric constants than surrounding flows. Many of the variations in reflectivity seen in Goldstone data, such as the bright flow margins, are at too fine a scale to be detected in Magellan altimetry-derived data.

Analysis of the set of parameters acquired by the two radar systems for several terrain types indicates that v ariat ions in dielectric constant are overwhelmed by wavelength-scale roughness variations in Magellan SAR data over plains regions. In Goldstone small-incidence-angle data, however, dielectric differences exert an important control on backscatter strength (e.g., parabolic features). Goldstone and Magellan data provide reasonably well-calibrated data at widely separated points on the scattering "law" for a number of Venus terrain types. Combining these types of data provides a more complete picture of the mechanisms of surface scattering. Comparison with rough surface scattering models and SAR observations of terrestrial surfaces indicates that the roughness characteristics of the equatorial plains and ridge belt surfaces are comparable to modified terrestrial lava flows, while the low-

backscatter parabolic feature is similar in roughness to gravel or fine tephra deposits.

Calibrated Earth-based radar observations have proven to be a useful complement to the orbital data acquired by Magellan. Future activities in this area could include targeting features in high-resolution mode for analysis of surface properties and change detection. Earth-based polarimetric measurements arc also an important complement to existing datasets [e.g., Campbell and Campbell, this issue]. Reduction and calibration of data already in hand, as well as data acquired in future experiments, will prove to be valuable components of ongoing studies of the surface of the planet.

Acknowledgments. The authors thank John Harmon and an anonymous reviewer for their comments. Thanks also to R. Jurgens and J. van Zyl for useful discussions. Parts of the research described herein were carried out at the Jet Propulsion Laboratory, California Institute of Technology, under contract from NASA. JJP was supported by the National Research Council under the Research Associateship Program. REA was supported by JPL contract 957415.

REFERENCES

Arvidson, R.Ft., J.J. Plaut, R.F. Jurgens, R.S. Saunders, arrd M.A. Slade, Geology of southern Guinevere Planitia, Venus, based on analyses of Goldstone radar data, *Proc. Lunar Planet Sci. Conf., 20th* 557-572, 1990.

Arvidson, R. E., V.R. Baker, C. Elachi, R.S. Saunders and J.A. Wood, Magellan: Initial analysis of Venus" surface modification, *Science*, 252, 270-275, 1991.

Asimow, P., and J.A. Wood, Fluid outflows from Venus impact craters: Analysis from Magellan data, *J. Geophys. Res.*, this issue.

Campbell, B.A. and D.B. Campbell, Analysis of volcanic surface morphology on Venus from comparison of Arccibo, Magellan and terrestrial airborne radar data, *J. Geophys. Res.*, this issue,

Campbell, D. B., N.J. Stacy, R.E. Arvidsorr, E.M. Jones, W.I. Newman, G.S. Musser, A.Y. Roper, and C. Schaller, Magellan observations of extended impact crater features on Venus, *J. Geophys. Res.*, this issue.

Campbell, M. J., and J. Ulrichs, Electrical properties of rocks and their significance for lunar radar observations. *J. Geophys. Res.*, 74. 5867-5881, 1969.

Hagfors, T., Remote probing of the moon by infrared and microwave emissions and by radar, *Radio Sci., 5,* 189-227, 1970.

Jurgens, R. F., R.M. Goldstein, H.R. Rumsey, and R.R. Green, Images of Venus by three-station interferometry: 1977 results, *J. Geophys. Res.*, 85, 8282-8294, 1980.

Jurgens, R. F., M.A. Slade, L, Robinett, S. Brokl, G.S. Downs, C. Franck, G.A. Morris, K, II. Farazian, and R.P. Chan, High resolution images of Venus from ground-based molar, *Geophys. Res. Lett., 15,* 577-580, 1988a,

Jurgens, R. F., M.A. Slade, and R.S. Saunders, Evidence for highly reflective materials on the surface and subsurface of Venus, Science, 240, 1021-1023, 1988b.

Pettengill, G.H., P.G. Ford, and B.D. Chapman, Venus: Surface electromagnetic properties, *J. Geophys. Res.*, 93, 14,881-14,892, 1988.

Pettengill, G. H., P.G. Ford, W.T.K. Johnson, R.K. Raney, and L.A. Soderblom, Magellan: Radar performance and data products, Science 252, 260-265, 1991.

Pettengill, G.H., P.G. Ford, and R.J. Wilt, Venus surface radiothermal emission as observed by Magellan, *J. Geophys. Res.*, this issue.

Plaut, J. J., Radar scattering as a source of geological information on Venus and Earth, Ph.D. thesis, Dep. of Earth and Planet. Sci., Washington Univ., St. Louis, Me., 1991.

Plaut, J.J., R.E. Arvidson, and R.F. Jurgens, Radar characteristics of the equatorial plains of Venus from Goldstone observations: Implications for interpretation of Magellan data, *Geophys. Res. Lett.*, 17, 1357-1360, 1990.

Plaut, J. J., R. Il. Arvidson, E.R. Stofan, and P.C. Fisher, Radar properties in the equatorial plains of Venus - Influence of impact, volcanic and tectonic features (abstract), *Lunar Planet Sci., XX//, 1073-1074, 1991.*

Rumsey, H.C., G.A. Morns, R.R. Green, and R.M. Goldstein, A radar brightness and altitude image of a portion of Venus, Icarus, 23, 1-7, 1974.

Squyres, S.W., D.M. Jams, G. Baer, D.L. Bindschadler, G. Schubert, V. I.. Sharpton, and E.R. Stofan, The morphology and evolution of coronae on Venus, *J. Geophys. Res.*, this issue.

Ulaby, F.T., T. I{. Bengal, M.C. Dobson, J.R. East, J.B. Garvin, and D. I.. Evans, Microwave dielectric properties of dry rocks, *IEEE Trans. Geosci. Remote Sens.*, 28, 325-336, 1990.

Ulaby, F.T., R.K. Moore, and A.K. Fung, *Microwave Remote Sensing Active and Passive,* vol. II, Addison-Wesley Publishing, Reading, Mass., 1982.

van Zyl, J. J., H.A. Zebker, and C. Elachi, Imaging radar polarization signatures: Theory and observation, *Radio Sci., 22, 529-543, 1987.*

Fig. 1. Magellan SAR mosaic with locations of Goldstone observations 1972-1988 outlined in white. Latitude range 23°S to 23°N, longitude range 260°E to 32°E. North-south dimension is approximately 4800 km. Large gaps in center of image are areas of thermally constrained mapping passes. Disrupted zones in west are southern Devana Chasma and Phoebe Regio; Heng-O corona is at right center.

Fig. 1. Magellan SAR mosaic with locations of Goldstone observations 1972-1988 outlined in white. Latitude range 23°S so 23°N, longitude range 260°E to 32°E. North-south dimension is approximately 4800 km. Large gaps in center of image are areas of thermally constrained mapping passes. Disrupted zones in west are southern Devana Chasma and Phoebe Regio; Heng-O corona is at right center.

Fig. 2a. Goldstone backscatter image of northeast Heng-O corona, Topographic sensitivity at Gold stone incidence angles emphasizes corona rim and interior structures. Floor and rim of 35-km-diameter Hellman crater at center left are displaced in Goldstone image due to projection of data into range space under the assumption of a spherical surface. Goldstone data from July 7, 1988. Image dimensions arc 950 km x 950 km. Center coordinates are 4.1°N, 357.1°E. Goldstone incidence angle range 0.5°-4.50.

Fig. 2b. Magellan SAR image of same area as Figure 2a. Note contrast reversals bctwccn the images on impact crater materials and linear fracture sets in corona interior,

Fig. 3a. Goldstone backscatter image of Heng-O corona and she adjacent low-emissivity impact-related parabolic feature. Arrow in Figure 3b indicates position of impact crater. Goldstone data from July 11, 1980. Image dimensions are 1470 km x 1470 km. Center coordinates are 4.4°N, 356.9°E. Goldstone incidence angle range 1.5"-7.2°.

Fig. 3b. Magellan emissivity data for same area as Figure 3a. Emissivity values on the impact-related feature are .-0.035 lower than the surroundings. The strong correlation of details in the feature between Goldstone and emissivity data implies higher dielectric constants, while poorer correlation with Magellan SAR argues against a roughness control on emissivity for this "parabola".

Fig. 3c. Magellan SAR backscatter image of same area as Figure 3a.

Fig. 4a. Gold stone backscatter image of volcanic terrain in central Navka Planitia. Compare with Magellan SAR image in Figure 4b. Complex contrast relationships are seen on lava flows and domes in northern half of the images. Flow at 1 is brighter than surrounding plains in troth images, while flow at 2 has reversed contrast relative to the plains. Dome at 3 has very low backscatter in Goldstone data relative to the adjacent flow to the south, while little contrast is seen in Magellan image. Bright flow margins at 4 in Goldstone data are not discernible in Magellan SAR, implying uniform flow roughness at the wavelength scale, but an increase in bulk density at the margins. Goldstone data from March 18,1977. Image dimensions are 1500 km x 1500 km. Center coordinates are 8.4°S, 3 10.2°E. Goldstone incidence angle range 1.5°-7.20.

Fig. 4b. Magellan SAR backscatter image of same area as Figure 4a,

Fig. 5. Specific radar cross section, σ^0, as a function of incidence angle for the three surfaces in Table 2. Also plotted for reference are three models of scattering behavior. Hagfors function parameters are global mean values of uncorrected Fresnel reflection coefficient, 0.109, and rms slope, 2.77°. Muhleman law approximates the average scattering behavior at large angles [Pettengill et al., 1988]. Small perturbation model parameters: real dielectric constant of 4.3, exponential autocorrelation function with rrns height of 2.0 cm. Absolute errors assigned to Goldstone values are ± 1.5 dB, to Magellan values ± 3 dB.

[1]Jet Propulsion Laboratory, Pasadena, California.
[2]Department of Earth and Planetary Sciences, Washington University, Saint Louis, Missouri,

Paper number 92JE01439.
0148 -0227/92/92JE01439$05 .00

R.E. Arvidson, Department of Earth and Planetary Sciences, Washington University, Campus Box 1169, One Brookings Drive, St. Louis, MO 63130-4899.
J.J. Plaut, MS 230-225, Jet Propulsion Laboratory, 4800 Oak Grove Drive, Pasadena CA 91109.

(Received November 4, 1991;
revised June 17, 1992;
accepted June 22, 1992.)

TABLE 1. Characteristics of the Radar Systems

	Wavelength, cm	Resolution	Incidence Angle	Polarization
Goldstone	12.6 (pre-1976) 12.9 (post-1976)	1-10 km	0°-7"	OC (oppposite circular)
Magellan SAR	12.6	20-360 m	17°-450	HH (horizontal transmit & receive)
Magellan altimetry	12.6	7-29 km	0°-10"	HH
Magellan radiometry	12.6	16-87 km	17°-450	H (receive only)

TABLE 2. Radar Scattering and Emission Properties of Selected Surfaces

Unit	Latitude	Longitude	Goldstone: Date	θ	σ°	Po	rms	Magellan: e	σ°	ρ0	ρ0'	rms	Emiss.
Plains	10	0	July 11, 19S0	6.3	-1.54	0.061	3.9	44	-14.7	0.076	0.091	1.7	0.829
Parabola	10	359	July 11, 1980	5.9	236	0.106	2.8	44	-17.1	0.116	0.122	2.6	0.790
Ridge belt	-4	341	Feb. 04, 1982	6.3	-0.25	0.053	4.3	44	-14.4	0.048	0.067	3.9	0.869

θ, incidence angle, degrees; u", specific radar cross section in decibels; ρ_0, Fresnel reflection coefficient; rms, root-mean-square slope, degrees; ρ_0', Fresnel reflection coefficient corrected for diffuse scattering; Emiss., emissivity.

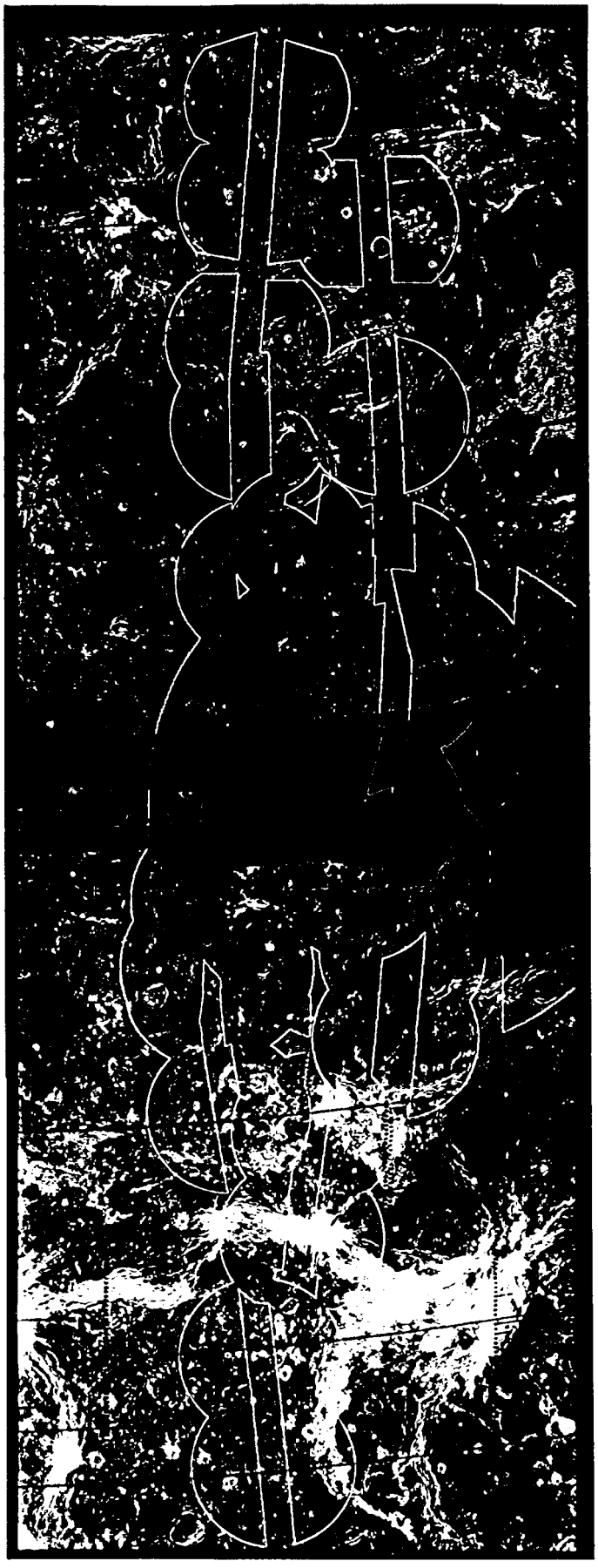

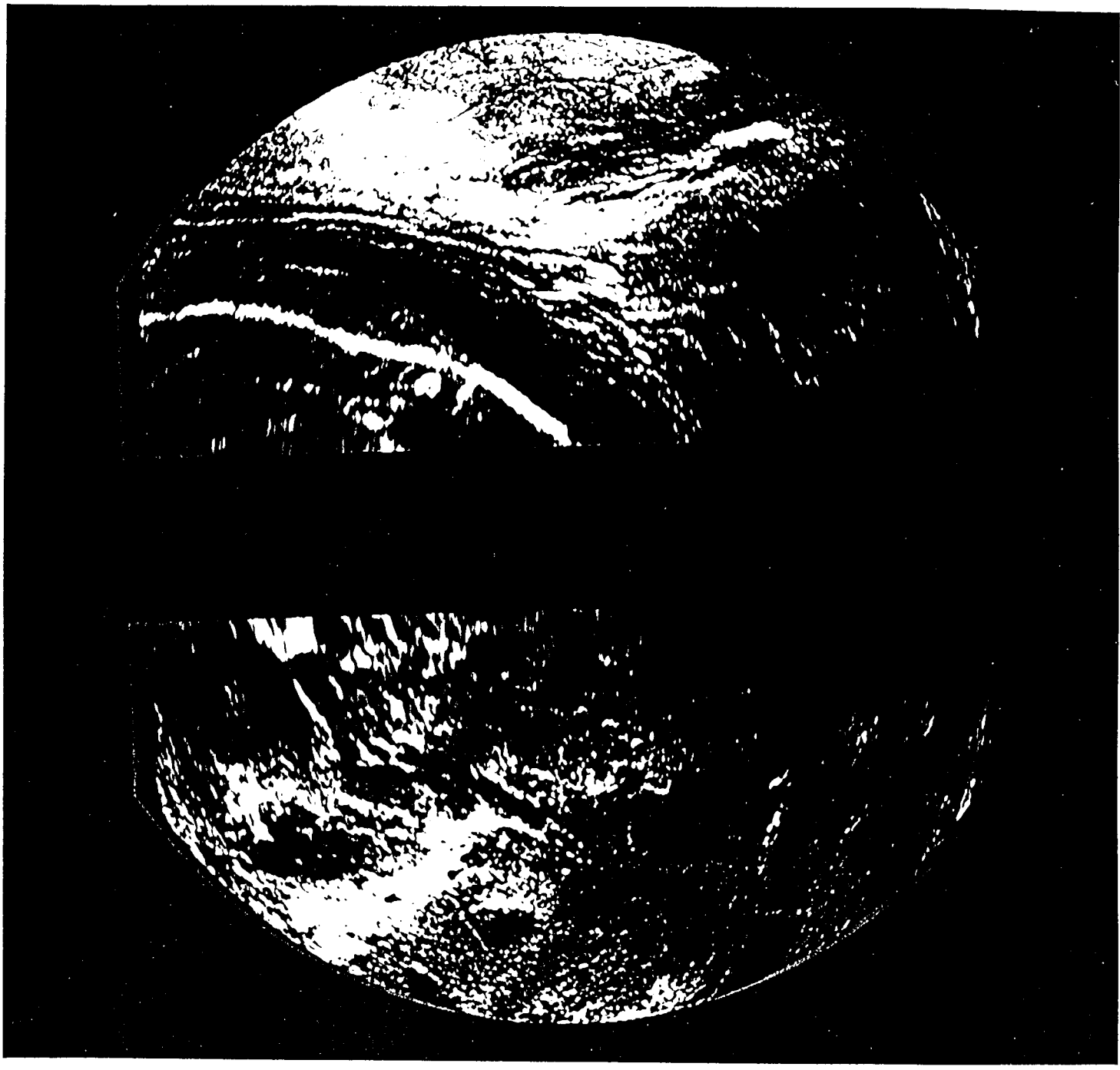

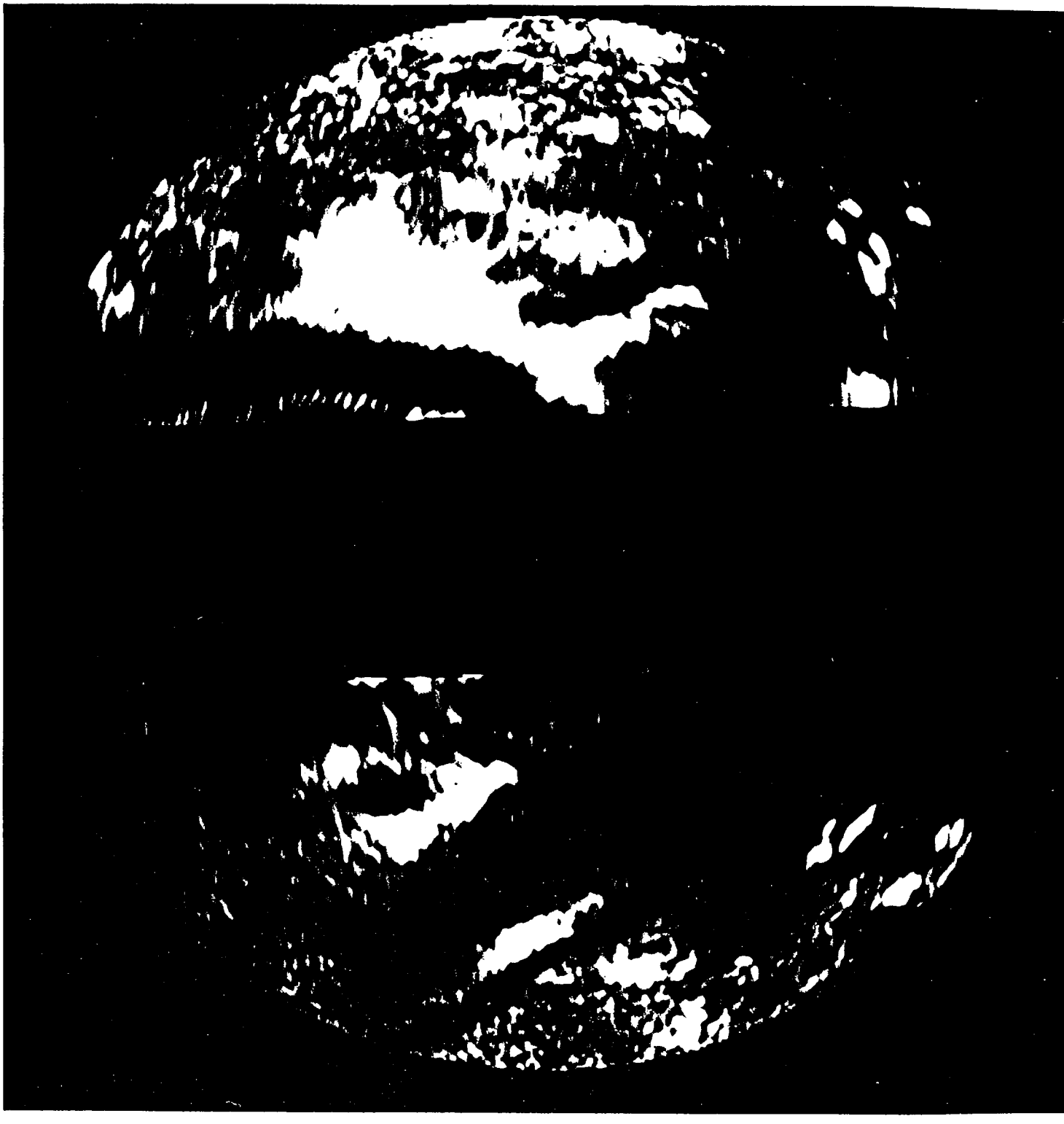

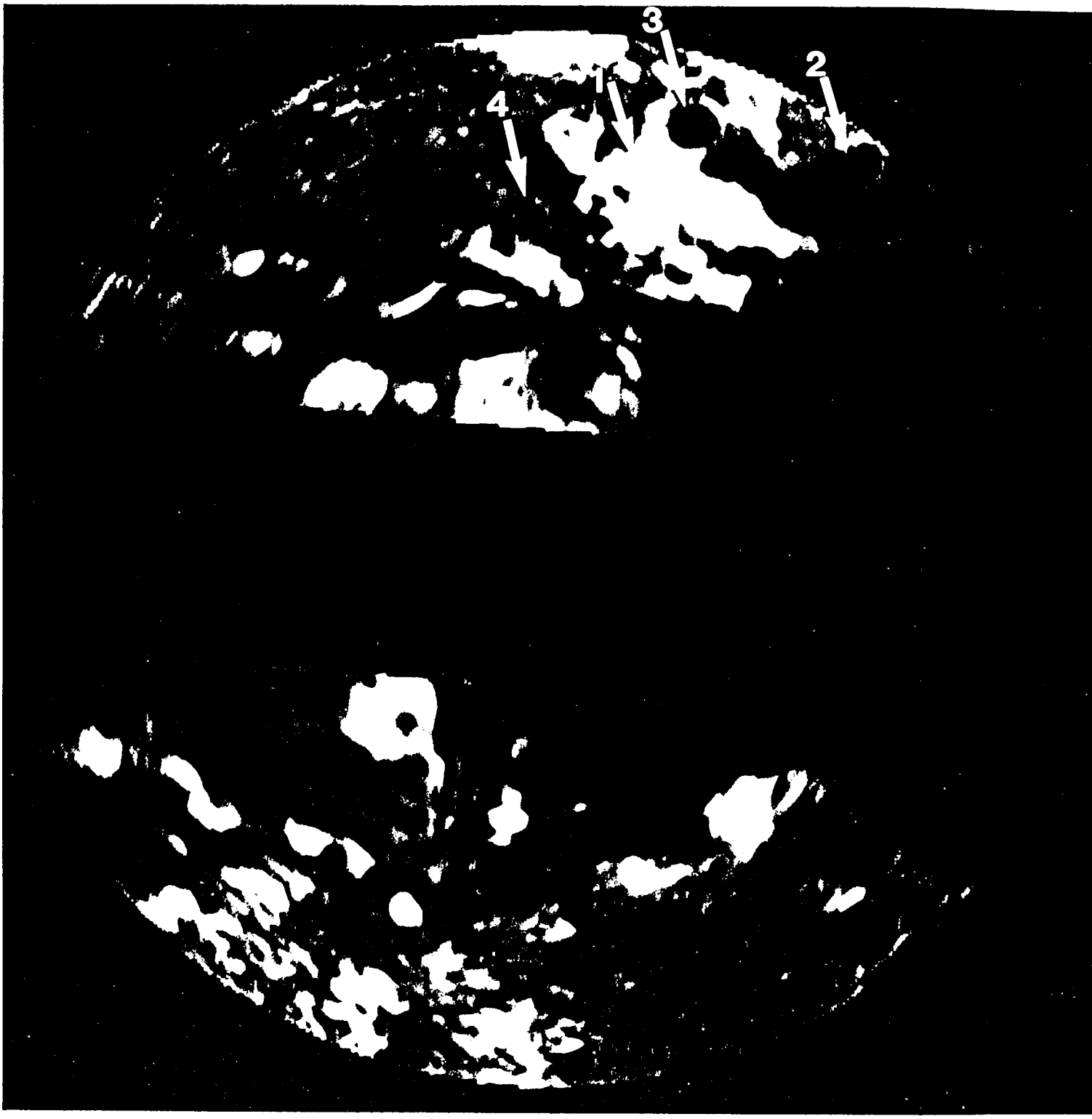
3
2
1
4

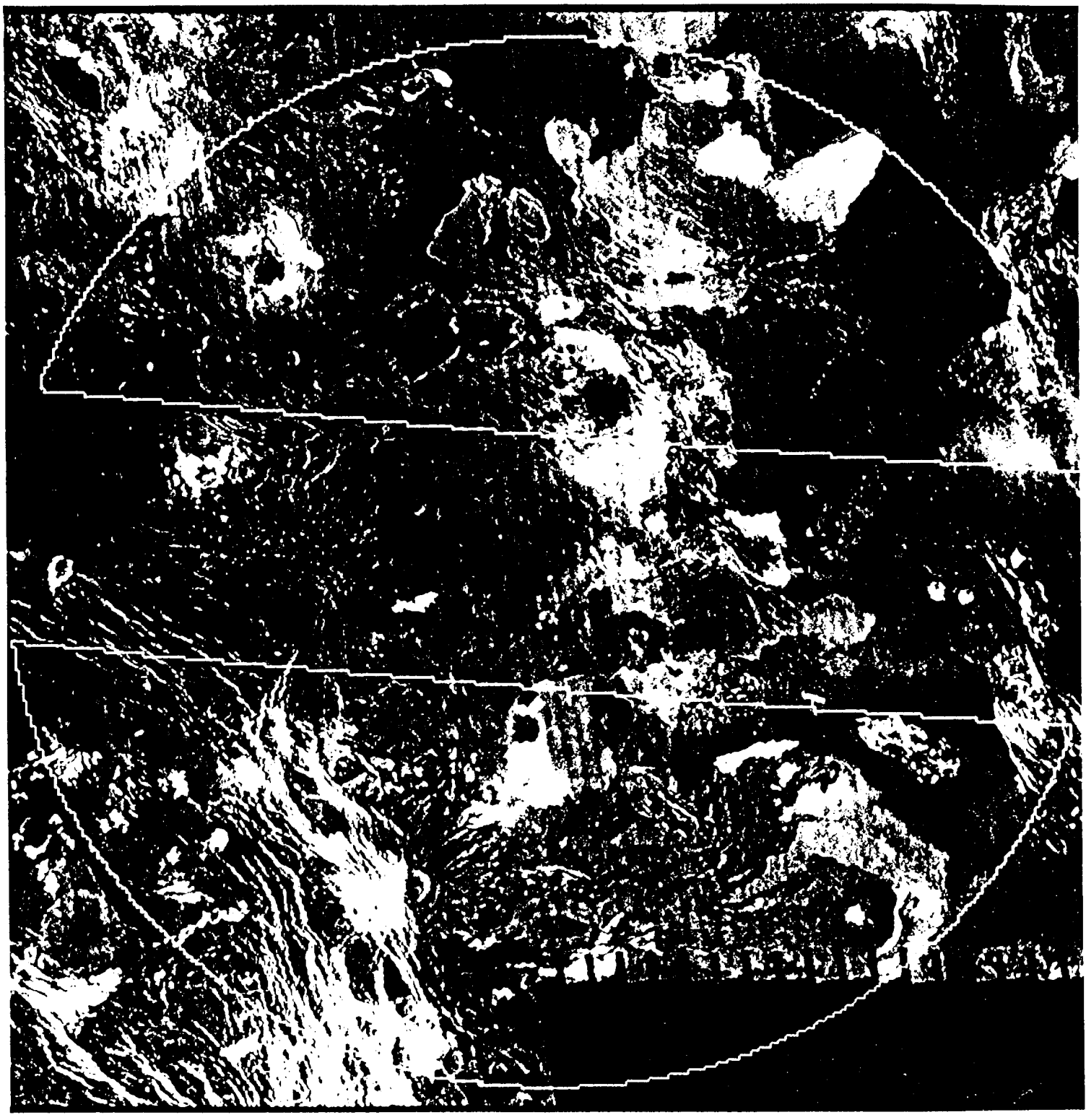

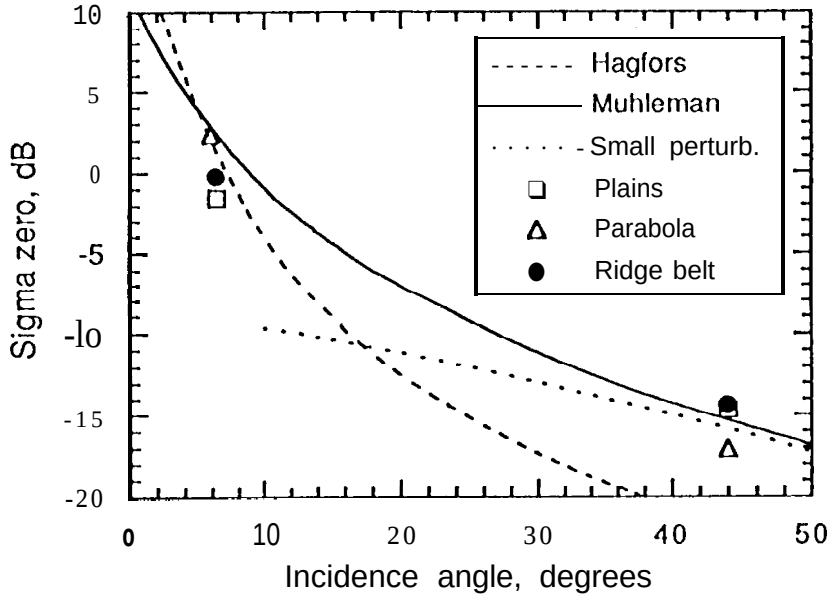

Plaut and Arvidson, Figure 5